Figure 3. At critical conditions the osmotic compressibility goes to infinity and then suddenly drops to substantially low values as shown by the dashed curve. However, the present theory also predicts an increased sensitivity of κ_{os} on v_2 slightly before critical conditions are attained (the solid curve in Figure 3). These predictions are in qualitative agreement with recent experiments[21] carried out in the vicinity of the Θ temperature with PVAc in isopropyl alcohol. The apparent exponent m is reported to vary between 2.31 and 13.3, though no collapse of the gel systems is observed.[21]

According to eq 32 and 33, the slope of the line log v_2/K_v vs. log v_2 must be equal to −1.25. The experimentally observed[7] values exhibit a slope equal to −1.4. Zrinyi and Horkay argue[7] that this slope is substantially larger than the value of −1 predicted by the mean field formalism but rather approaches the value of −1.25 predicted by scaling laws. The exponent −1 deduced from the mean field formalism is based on the truncation of the series expansion of the logarithmic term in eq 22 after the first term. As was pointed out recently,[16] the representation of the combinatory portion of the chemical potential by the truncated virial series is not acceptable unless a manageable number of terms are kept. The terms with powers of v_2 exceeding 1 cannot be neglected, particularly in the semidilute domain. The present work demonstrates that by proper treatment of the theory, i.e., by retention of the logarithmic term and suitable choice of the concentration dependence of the χ parameter, the experimental results are exactly reproducible. The convergence to the slope −1 occurs only in the limit as $v_2 \to 0$, as the slight curvature of the theoretically obtained curve in Figure 4 indicates.

Acknowledgment. B.E. gratefully acknowledges the hospitality and financial support of IBM Research, San Jose, CA, where the present work was initiated in collaboration with Prof. P. J. Flory in the summer of 1985.

Registry No. PVAc, 9003-20-7.

References and Notes

(1) Flory, P. J.; Rehner, J. *J. Chem. Phys.* **1944**, *12*, 412.
(2) Gee, G. *Trans. Faraday Soc.* **1946**, *42B*, 33.
(3) Treloar, L. R. G. *The Physics of Rubber Elasticity*, 3rd ed.; Clarendon Press: Oxford, 1958.
(4) Treloar, L. R. G. *Trans. Faraday Soc.* **1950**, *46*, 783.
(5) Flory, P. J.; Tatara, Y. *J. Polym. Sci., Polym. Phys. Ed.* **1975**, *13*, 683.
(6) See, for example: Candau, S. J.; Young, C. Y.; Tanaka, T.; Lemarechal, P.; Bastide, J. *J. Chem. Phys.* **1979**, *70*, 4694. Hecht, A. M.; Geissler, E. *J. Phys. (Les Ulis, Fr.)* **1978**, *39*, 631. Geissler, E.; Hecht, A. M. *J. Phys. (Les Ulis, Fr.)* **1978**, *39*, 955. Geissler, E.; Hecht, A. M. *Macromolecules* **1980**, *13*, 1276; *ibid.*, **1981**, *14*, 185. Bastide, J.; Candau, S.; Leibler, L. *Macromolecules* **1981**, *14*, 719. Belkebir-Mrani, A.; Beinert, G.; Herz, J.; Rempp, P. *Eur. Polym. J.* **1977**, *13*, 277. Horkay, F.; Zrinyi, M. *Macromolecules* **1982**, *15*, 1306 and references cited therein.
(7) Zrinyi, M.; Horkay, F. *J. Polym. Sci., Polym. Phys. Ed.* **1982**, *20*, 815.
(8) Flory, P. J. *Trans. Faraday Soc.* **1961**, *57*, 829.
(9) In the literature the osmotic compressibility is also defined[7] as $\kappa_{os} = -\bar{V}_1/(\partial\Delta\mu_1/\partial v_2)$. The bulk modulus is then related to κ_{os} by the relation $K_v = v_2/\kappa_{os}$.
(10) Flory, P. J. *Discuss. Faraday Soc.* **1970**, *49*, 7 and references cited therein.
(11) Koningsveld, R.; Kleintjens, L. A.; Schoffeleers, H. M. *Pure Appl. Chem.* **1974**, *39*, 1.
(12) Flory, P. J. *J. Chem. Phys.* **1977**, *66*, 5720.
(13) Flory, P. J. *Polym. J. (Tokyo)* **1985**, *17*, 1.
(14) Flory, P. J. *Br. Polym. J.* **1985**, *17*, 96. Erman, B. *Br. Polym. J.* **1985**, *17*, 140.
(15) Erman, B.; Flory, P. J. *Macromolecules* **1983**, *16*, 1607.
(16) Erman, B.; Flory, P. J. *Macromolecules* **1986**, *19*, 2342.
(17) Flory, P. J.; Erman, B. *Macromolecules* **1982**, *15*, 800.
(18) Browning, G. V.; Ferry, J. D. *J. Chem. Phys.* **1949**, *17*, 2805.
(19) de Gennes, P.-G. *Scaling Concepts in Polymer Physics*; Cornell University Press: Ithaca, NY, and London, 1980.
(20) Flory, P. J. *Principles of Polymer* Chemistry; Cornell University Press: Ithaca, NY, 1953.
(21) Zrinyi, M.; Horkay, F. *Macromolecules* **1984**, *17*, 2805.

Two-Dimensional NMR Determination of the Conformation of an Alternating Styrene–Methyl Methacrylate Copolymer

Peter A. Mirau,* Frank A. Bovey, Alan E. Tonelli, and Sharon A. Heffner

AT&T Bell Laboratories, Murray Hill, New Jersey 07974. *Received January 9, 1987*

ABSTRACT: Two-dimensional nuclear Overhauser effects (2D NOE) have been used to study the solution conformation of a strictly alternating styrene–methyl methacrylate copolymer. The average solution conformation is determined by measuring the strength of the dipolar interaction between the methylene protons on the polymer main chain from the rate of buildup and decay of the cross peaks in the 2D NOE spectrum. These rates are inversely proportional to the sixth power of the internuclear distance and are therefore sensitive to the local conformation. The NMR-determined average conformation for the styrene units in cohetero triads is 58 ± 5% tt, 24 ± 5% tg^-, and 18 ± 5% g^+t with the isomeric states distorted by 11° from perfectly staggered to accommodate the bulky phenyl groups. These values are compared with those calculated from rotational isomeric state models.

Introduction

Predicting the macroscopic properties of polymers requires an understanding of their structural and dynamic properties at a molecular level and has been the focus of intensive research. It is experimentally difficult, however, to study the molecular behavior of polymer chains at a local level, and indirect methods are frequently employed.[1,2] Measurements of end-to-end distances or dipole moments are examples of indirect means by which one may hope to deduce local properties—principally bond rotational states—by comparison with theoretical predictions from rotational isomeric state models.[3]

NMR has been extensively employed to determine the structure and dynamics of polymers both in solution and in the solid state.[4,5] Proton NMR has made major contributions to our understanding of the microstructure of synthetic polymers, but during the past 15 years had been largely eclipsed by carbon-13 NMR because of the much greater range of carbon chemical shifts and the corresponding greater sensitivity to structural detail. Proton

0024-9297/87/2220-1701$01.50/0

Chart I

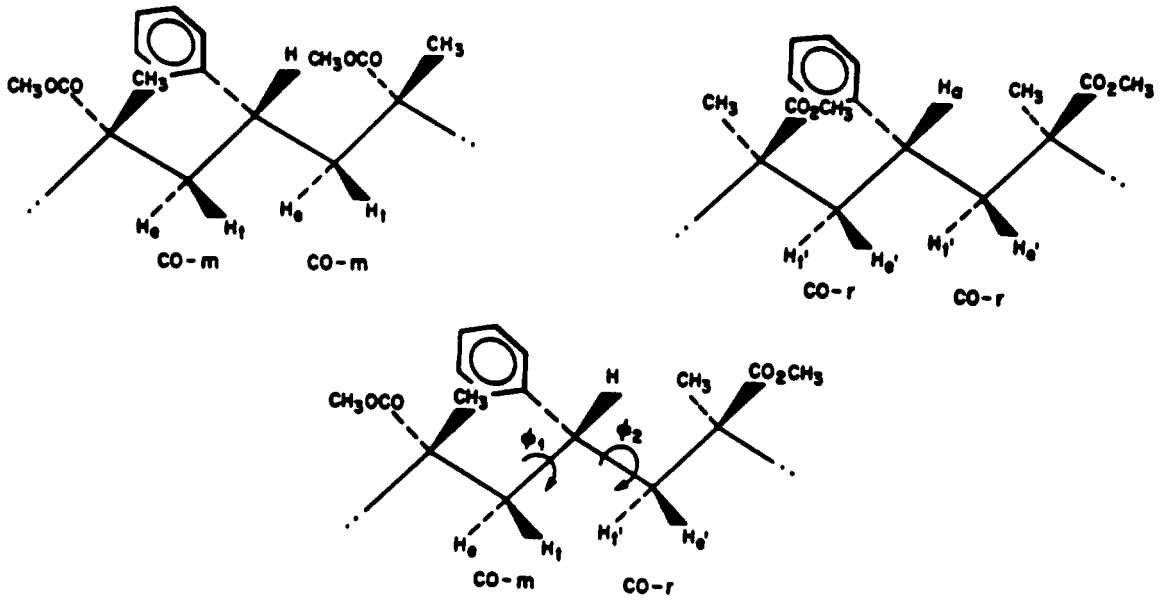

NMR has certain inherent advantages, however. Among these are much more rapid spectral acquisition, the ability to measure J couplings, which may in turn be related to conformation, and the ability to provide fundamental symmetry information. These features have encouraged a renaissance in its use for the observation of synthetic polymers, particularly in two-dimensional (2D) NMR.[6-9] It has never fallen out of fashion in the study of biological molecules.

Structural information is normally obtained from proton NMR by observation of chemical shifts and J couplings. Even more detailed and precise information may be obtained by nuclear relaxation measurements, which provide not only correlation times but also, through nuclear Overhauser effects, interproton distances.[1,2] This method has seen very limited application to certain rigid biological molecules (proflavin,[10] gramicidin,[11] cyclic peptides,[12] proteins,[13] and nucleic acids[14]) but none to flexible chains existing in several interchanging conformations, the normal state of most synthetic polymers. We have described the qualitative application of 2D proton NMR to a 1:1 alternating styrene–methyl methacrylate copolymer.[15] In this paper we extend this treatment to a quantitative investigation of the solution conformation of this polymer.

Methods and Materials

The alternating styrene–methyl methacrylate copolymer was prepared as previously described.[15] NMR experiments were performed at 500 MHz using a JEOL GX-500 spectrometer on a 10% solution of the copolymer at 65 °C in a mixture of hexachlorobutadiene and deuteriated benzene. Pure absorption-phase 2D nuclear Overhauser effects (2D NOE) were measured by the method of States et al.,[16] using the $\pi/2$–t_1–$\pi/2$–τ_m–$\pi/2$–t_2 pulse sequence. The pulse phases were cycled to remove the cross-peak contributions from single and double quantum coherences due to J couplings.[17,18] Zero quantum coherences were not removed by this procedure but were ignored because they are dispersive in character and do not contribute to the cross-peak volumes.[19] A total of 256 t_1 increments (16 scans, 2K points) were acquired for each 2D data set and the matrix was zero-filled to a final size of 2K × 1K. One-hertz line broadening was applied in each dimension prior to Fourier transformation. Diagonal and cross-peak volumes were obtained by integrating slices through the 2D spectrum.

Results

Alternating Styrene–Methyl Methacrylate Copolymers. The synthesis of the strictly alternating styrene–methyl methacrylate copolymer and its characterization by 1D and 2D NMR has been previously reported.[15,20-22] Figure 1 shows the 500-MHz proton spectrum of the copolymer along with the assignments of the proton resonances obtained from these studies. The spectrum is simpler and seemingly more highly resolved than that of the 1:1 random styrene–methyl methacrylate copolymer due to the restriction of the possible sequences.[22] The methyl and methoxy resonances are resolved into three peaks due to the co-iso, co-hetero, and co-syndio configurations (Chart I). The geminal methylene protons are well separated from each other, and separate peaks are observed for the co-meso and co-racemic protons. These protons are designated H_e and H_t in the meso dyads and $H_{e'}$ and $H_{t'}$ in the racemic ones; this nomenclature is an extension of that used for poly(methyl methacrylate).[15,23]

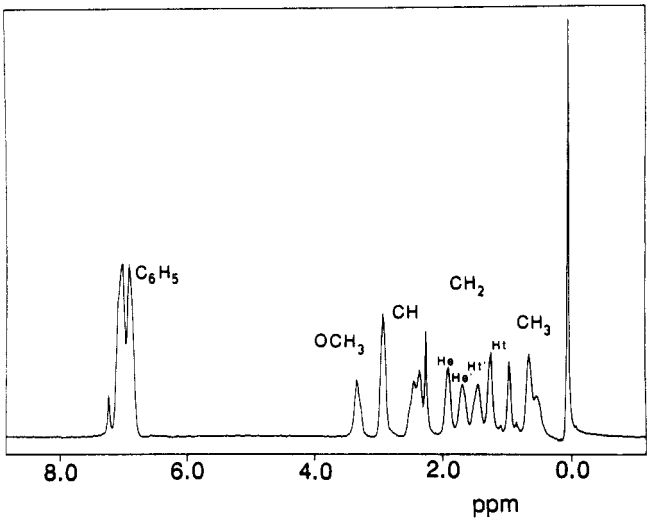

Figure 1. 500-MHz proton NMR spectrum of the 1:1 styrene–methyl methacrylate copolymer in 90% hexachlorobutadiene/10% deuteriobenzene at 65 °C.

2D NOE Studies. A 2D NOE spectrum consists of peaks lying along the diagonal and peaks connecting the diagonal peaks (cross peaks). The diagonal peaks are frequently the most intense features in the spectrum and arise from that portion of magnetization precessing at the same frequency during the t_1 and t_2 periods. Distance information is obtained from the analysis of the smaller

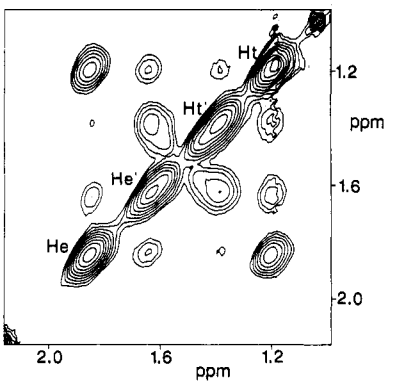

Figure 2. 500-MHz 2D NOE spectrum of the styrene–methyl methacrylate copolymer at 65 °C. This part of the 2D spectrum shows the interactions between the methylene protons and was obtained with a mixing time of 0.2 s.

cross peaks due to the magnetization transferred during the mixing time (τ_m).

The 2D NOE spectrum of the alternating styrene–methyl methacrylate copolymer shows a number of cross peaks connecting resonances within a monomer unit and connecting the neighboring units.[15] The intensities of the diagonal and cross peaks vary as a function of mixing time and depend on the molecular motions and the inverse sixth power of the proton–proton separation.[10-14,17,18] Many of these cross peaks have been used to characterize the copolymer, as they depend on the chemical structure and stereochemistry.[15] In this study we focus on the interaction between the methylene protons, as the strength of this interaction depends most strongly on the average solution conformation. Figure 2 shows a contour plot of the methylene region of the 2D NOE spectrum of the copolymer at 65 °C obtained with a 0.2-s mixing time. The strongest cross peaks arise from the nonequivalent geminal protons, the H_e–H_t and $H_{e'}$–$H_{t'}$ pairs. The distance separating the geminal protons is fixed at 1.80 Å and does not depend on the conformational properties of the copolymer. There are a number of weaker cross peaks in Figure 2 arising from interactions between the H_e–$H_{e'}$, H_e–$H_{t'}$, $H_{e'}$–H_t, and $H_{t'}$–H_t protons. Since we can observe interactions only for those protons with different chemical shifts,[17,18] the 2D NOE spectrum reports on only a fraction of the proton–proton interactions. Interactions between neighboring co-meso or co-racemic dyads cannot be observed; only meso–racemic interactions (the co-hetero sequences) give rise to methylene cross peaks in the 2D spectrum.

Figure 3 shows slices through the 2D NOE spectrum (0.2-s mixing time) at the frequencies of the four resolved methylene protons. The most intense peaks correspond to the resonances along the diagonal, and the weaker signals are the cross peaks. Peak volumes required for analysis of the cross relaxation rates are obtained by integrating the peaks in several slices. These plots clearly show the relative strength of the geminal (e.g., bottom, the H_e–H_t cross peak) and the vicinal interactions (e.g., bottom, the H_e–$H_{e'}$ cross peak).

Peak Intensity vs. Mixing Time. The strength of the dipolar interactions can be determined by measuring the intensity of the diagonal and cross peaks in the 2D NOE experiment as a function of the mixing time.[10-14,17-19,24-29] At short mixing times the diagonal peaks are intense and the cross peaks are absent. At longer mixing times the diagonal peaks decay while the cross peaks increase in intensity, and, at very long mixing times, all peak intensities decrease due to spin–lattice relaxation. The growth and decay of the methylene cross-peak volumes as a function of mixing time are shown in Figure 4. At the shortest mixing time (0.02 s) only the very strong geminal interactions lead to observable cross peaks. As the mixing time increases, the geminal cross peaks (H_e–H_t and $H_{e'}$–$H_{t'}$) build up to a maximum NOE of 12% at 0.2 s. At mixing times longer than 0.05 s, the other methylene cross peaks become visible and reach a maximum of 3–6%. The peak volumes measured at each mixing time can be used to solve for the elements of the relaxation rate matrix (vide infra), and the solid lines in Figure 4 show the predicted time course of the cross-peak volumes using the average of the rates measured in the six 2D NOE experiments.

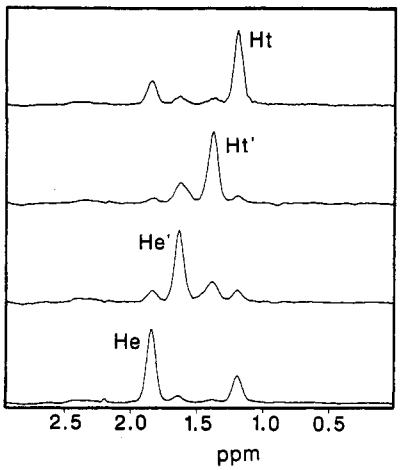

Figure 3. Slices through the 2D NOE spectrum shown in Figure 2. The four slices were taken at the frequencies of the H_e, $H_{e'}$, $H_{t'}$, and H_t protons.

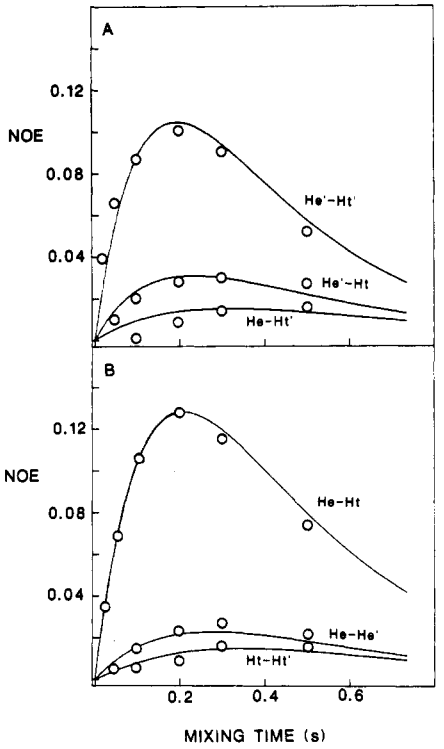

Figure 4. Time dependence of the cross-peak intensities as a function of mixing time. The data are shown for (A) $H_{e'}$–$H_{t'}$, $H_{e'}$–H_t, and H_e–$H_{t'}$ and for (B) H_e–H_t, H_e–$H_{e'}$, and $H_{t'}$–H_t. The solid lines show the time dependence of the cross peaks as calculated from the average values in the relaxation rate matrix. See text for details.

Analysis of NOE Peak Volumes. Several approaches may be used to extract cross relaxation rates from 2D NOE data as a function of the mixing time. The simplest analysis assumes that a multispin system such as the co-

polymer can be treated as a collection of isolated two-spin systems.[17,18] The cross relaxation rates are then obtained by measuring only the initial buildup of cross-peak volumes. This approach is difficult when, as with the copolymer, the cross peaks are small at short mixing times. The next level of sophistication is to fit the cross-peak buildup and decay throughout the entire range of mixing times.[24,25] This avoids the problem of measuring the small initial peak volumes but assumes that none of the cross peak intensity is due to indirect transfer of magnetization.[17,18] Such indirect transfer is possible in our system because of the strongly coupled geminal protons. In this study we analyzed the cross-peak volumes to obtain the cross relaxation rates by numerically solving the coupled differential equations describing the transfer of magnetization between the spins.[17,26-29] This approach is the most rigorous and makes no assumptions about indirect spin transfer.

The equation describing the dependence of the cross-peak volumes $\mathbf{A}(\tau_m)$ as a function of the mixing time (τ_m) is

$$\mathbf{A}(\tau_m) = \mathbf{A}_0 e^{-\mathbf{R}\tau_m} \tag{1}$$

where $\mathbf{A}_0$ are the peak volumes at zero mixing time and $\mathbf{R}$ is the matrix of relaxation rates which has the form[17,18]

$$\mathbf{R} = \begin{bmatrix} R_{ii} & \sigma_{ij} & \cdot & \cdot \\ \sigma_{ij} & R_{jj} & \cdot & \cdot \\ \cdot & \cdot & \cdot & \cdot \\ \cdot & \cdot & \cdot & \cdot \end{bmatrix} \tag{2}$$

The relaxation rates describing the time dependence of the diagonal ($i = j$) and off-diagonal ($i \neq j$) peaks can be written in terms of the spectral densities as

$$R_{i=j} = K\sum_{j=1}^{n} \frac{1}{r_{ij}^{-6}}\{J_0(0) + 3J_1(\omega) + 6J_2(2\omega)\} \tag{3}$$

and

$$\sigma_{ij} = K\frac{1}{r_{ij}^{-6}}\{6J_2(2\omega) - J_0(0)\} \tag{4}$$

where $K = \gamma^4\hbar/10$ and the spectral density terms (J_0, J_1, and J_2) depend on the molecular motions.[4,5,30,31] In the analysis of the copolymer it is not necessary to specify the spectral densities (vide infra). The rates along the diagonal are the same as those for a selective 1D relaxation rate measurement and the off-diagonal terms are the cross relaxation rates.[19] Since the cross relaxation depends on the relative spin populations of the interacting protons, the description of the spin system is a set of coupled differential equations. The experimentally measured peak volumes $\mathbf{A}(\tau_m)$ and the peak volumes at zero mixing time $\mathbf{A}_0$ can be used to solve for the elements of the relaxation rate matrix at each τ_m.[18,24-29] Equation 1 can be rewritten as

$$-\left(\frac{1}{\tau_m}\right) \ln\left\{\frac{\mathbf{A}(\tau_m)}{\mathbf{A}_0}\right\} = \mathbf{R} \tag{5}$$

This equation can be solved in terms of the matrix of eigenvectors χ and the diagonal matrix of eigenvalues $\mathbf{D}$ of $\ln \mathbf{A}(\tau_m)/\mathbf{A}_0$ as

$$\frac{\chi \ln \mathbf{D}\chi^{-1}}{\tau_m} = \mathbf{R} \tag{6}$$

The strategy in these experiments was to measure the peak volumes for several mixing times. The intensities of the diagonal peaks were then extrapolated to zero mixing time to obtain $\mathbf{A}_0$, and the relaxation matrix was then solved at each mixing time. The average diagonal and cross relaxation rates and the estimated errors are compiled in Tables I and II. The goodness of fit of these data is shown in Figure 4, where the solid lines are calculated from the average cross relaxation rates measured as a function of mixing time. The theoretical curves were obtained by starting with the average relaxation matrix and reversing the above procedure to obtain the cross-peak volumes as a function of mixing time. Part of the peak volumes plotted in Figure 4 are due to indirect spin transfer (spin diffusion);[27,28] the rates in Tables I and II are the rates for the direct through space transfer of magnetization.

Table I
Relaxation Rates for the Methylene Diagonal Peaks and the Geminal Methylene Cross Relaxation Rates

diagonal	σ_{ij},[c] s^{-1}	cross peaks[a]	σ_{ij},[c] s^{-1}
H_e	4.9 ± 0.3	H_e–H_t	−1.7 ± 0.4
$H_{e'}$	5.1 ± 0.2	$H_{e'}$–$H_{t'}$	−1.5 ± 0.3
$H_{t'}$	5.2 ± 0.3		
H_t	4.9 ± 0.2		

[a] Negative cross relaxation rates are found for molecules tumbling within the slow motion limit (i.e., for correlation times greater than 0.3 ns at 500 MHz) where the relaxation is dominated by J_0 (eq 4).

Table II
Methylene Cross Relaxation Rates and Estimated Proton–Proton Distances

interaction	σ_{ij},[c] s^{-1}	distance range,[a] Å
H_e–$H_{e'}$	−0.22 ± 0.06	2.41–2.65
H_e–$H_{t'}$	−0.13 ± 0.05	2.59–2.97
H_e–H_t	−0.32 ± 0.03	2.32–2.40
$H_{t'}$–H_t	−0.09 ± 0.02	2.82–3.04

[a] The calculated distances were corrected for the random stereochemistry of the copolymer. The distance range is calculated by adding and subtracting the standard deviation from the average distance. The data are presented in this way to illustrate the effect of the inverse sixth-power average on the estimated errors.

Proton–Proton Distances. The cross relaxation rates obtained from the 2D NOE analysis depend both on the inverse sixth power of the proton distance separations and on the spectral density terms. Calculation of the spectral densities is simple only for isotropic motion of the internuclear vectors. Many studies have shown, however, that the motions of polymer chains in solution are not isotropic, and a number of complex motional models have been used to relate NMR relaxation parameters to polymer dynamics.[30,31] Instead of modeling the spectral densities, we will assume that the dynamics of all the protons are similar and convert the cross relaxation rates into distance using the fixed geminal proton–proton separation as an internal reference. Any unknown distance can be calculated from the ratio of cross relaxation rates given by

$$\frac{\sigma_{ij}}{\sigma_{gem}} = \frac{r_{ij}^{-6}}{r_{gem}^{-6}} \tag{7}$$

where r_{gem} and r_{ij} are the geminal and unknown proton distances and σ_{gem} and σ_{ij} are their cross relaxation rates. The distances in the copolymer are calculated from the cross relaxation rate by assuming a geminal proton separation of 1.80 Å. The measured cross relaxation rates for the H_e–H_t and $H_{e'}$–$H_{t'}$ geminal interactions were −1.5 and −1.7 s^{-1} (Table I). This differences between meso and racemic proton cross relaxation rates may be related to variations in the dynamics of the two types of protons.[32] The average of the two rates was used in eq 7 to calculate the other proton–proton distances compiled in Table II. We must recognize that the polymer chain is not composed of isolated mr triads but is of random stereochemistry.

Chart II

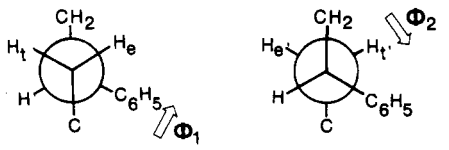

Table III
Dependence of the H–H Distances on the Rotational Isomeric State

	distance, Å		
interaction	*tt*	tg^-	g^+t
H_e–$H_{e'}$	3.09	2.58	3.71
H_e–$H_{t'}$	2.79	3.74	3.74
H_e–H_t	2.27	2.72	2.72
$H_{t'}$–H_t	3.10	3.71	2.58

Therefore, each m dyad in an mr triad has a 50% chance of having another m dyad in the unspecified position on the other side; these protons are identical and do not contribute to the cross-peak volumes. There is also a 50% chance of finding an r diad in this position, and this interaction does contribute. A parallel statement may be made with regard to the r dyad in the mr triad. It follows that the cross relaxation rates must be divided by 1.5 to take proper account of these additional interactions.

Distances in the Rotational Isomers. There is insufficient information in the measured distances to determine the solution structure a priori, so we use previous work on the solution structure of polymers to limit the number of possible conformational states that contribute to the average solution structure. On the basis of previous work on polystyrene and poly(methyl methacrylate), the three most likely isomers are the *tt*, tg^-, and g^+t; the other possibilities may be excluded due to their strong steric interactions (Chart II).[33-36] To determine the average structure, we take advantage of the fact that the proton–proton separations are different in the three isomers (Table III). For example, the $H_{e'}$–H_t distance is short (2.27 Å) in the *tt* isomer but relatively long (2.72 Å) in the tg^- and g^+t conformers. Therefore, if the measured $H_{e'}$–H_t distance is short, this means that the *tt* isomer is significantly populated in solution. If the distance is closer to 2.72 Å, then the average solution structure is predominately tg^- and g^+t. The closest H_e–$H_{e'}$ interaction occurs in the tg^- isomer, so a short H_e–$H_{e'}$ distance would indicate that the tg^- state was significantly populated in solution. In the g^+t state, the $H_{t'}$–H_t interaction is the strongest. Because of the nature of the experimental measurement, the distances are weighted by the sixth power, and the cross relaxation will be more heavily weighted with the shorter distances.

Angular deviations from perfectly staggered isomeric states are frequently observed for polymers with large substituent groups (Chart II). In consideration of this fact, we examined the distance dependence of the angular deviations from the perfectly staggered gauche and trans states. Figure 5 shows a plot of the proton–proton distances as a function of the distortion from perfect staggering in the *tt* isomer, assuming equal distortions for ϕ_1 and ϕ_2. The plot shows that some of the distances are sensitive to the distortion (H_e–H_t and H_e–$H_{t'}$) while others are not (H_e–$H_{e'}$ and $H_{t'}$–H_t). Unique distant dependent profiles are also obtained for the tg^- and g^+t states. In our analysis we searched for a combination of the populations of the states and the angular deviation that best fits the experimental distances.

Structural Constraints. The measurement of the proton–proton distances allows us to place constraints on

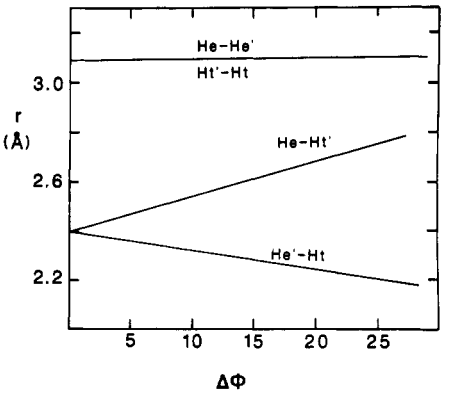

Figure 5. Effect of deviations of the torsional angles on the proton–proton distances in the *tt* rotational isomeric state.

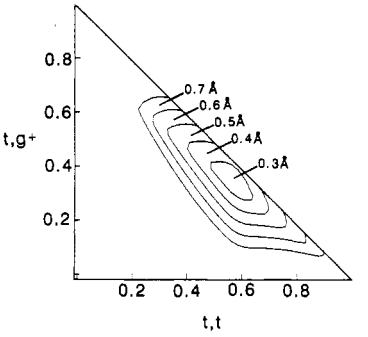

Figure 6. Plot showing the total difference between the NMR measured distances and those for a given combination of three isomeric states.

the possible solution conformation of the copolymer. While each distance is insufficient to characterize the conformation, all of the distance constraints together can be used to limit the possible structures in solution. To determine those combinations of the three states consistent with the NMR measured distances, we calculated the average distance expected for all four proton pairs for all combinations of *tt*, tg^-, and g^+t. The sixth-power average distance for any combination of the states is given by

$$\langle r^{-6} \rangle = f_{tt} r_{tt}^{-6} + f_{tg^-} r_{tg^-}^{-6} + f_{g^+t} r_{g^+t}^{-6} \qquad (8)$$

where f is the fraction of the state and r is the distance separating the proton pair. The comparison of the observed and calculated distance is made for the four proton pairs as a function of the distortion from the perfectly staggered states. Those combinations predicting distances similar to the measured ones are considered likely candidates for the average solution conformation.

Figure 6 shows a graphical device to visualize the total constraints implied by the four measured distances. Since the average solution conformation is assumed to consist of three conformation states, the data can be plotted as a function of two of the states. The axes in Figure 6 are the populations of *tt* and g^+t contributing to the average solution conformation. For example, the point at 0.2*tt* and 0.3g^+t implies that the fraction of tg^- is 0.5. The contour data plotted in Figure 6 are the absolute value of the total difference between the observed distances and those calculated for the particular combination of the *tt*, g^+t, and tg^- states. The best agreement is found for an average solution structure which is predominately *tt*. Close agreement between the measured and calculated distances was found for an average solution conformation of 58% *tt*, 24% tg^-, and 18% g^+t. For this combination the total difference between the four measured distances and the

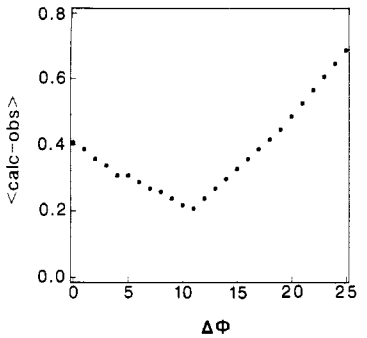

Figure 7. Dependence of the best fit on the deviation from the standard angles in the gauche and trans isomers. The calculations assume $\Delta\phi_1 = \Delta\phi_2$. See text and Chart II for details.

calculated ones was 0.21 Å. The contour plot in Figure 6 shows how the calculated distances diverge from the measured ones for other combinations of the states. If we consider a good fit to be that where the total difference is less than 0.3 Å, the area of best fit includes those structures within ±5% of the minimum. The populations determined by NMR differ in some respects from the rotational isomeric state (RIS) calculations of $0.53tt$, $0.20tg^-$, and $0.27g^+t$.[15] The agreement is good for the tt state, but the values for the other two fall outside of our region of best fit. The reason for this disagreement may be due to a number of different factors (solvent, etc.) and requires further investigation.

The goodness of agreement between the calculated distances and those measured by 2D NMR depends on the deviation from perfect gauche and trans states. Chart II shows Newman diagrams of the copolymers and illustrates how deviations from the gauche and trans may relieve the steric interactions. Figure 7 shows the dependence of the best agreement on the angular displacement from the perfect gauche and trans states assuming equal deviations for ϕ_1 and ϕ_2. The best agreement is found for a deviation of 11°; it is these data that are plotted in contour form in Figure 6. Figure 7 shows that the goodness of agreement decreases smoothly to 0.4 Å for perfectly staggered isomeric states. Poor agreement is found for deviations larger than 15°. Together these data show that NMR may provide a detailed picture of the solution structure of polymers in terms of both the population of rotational isomeric states and the deviations from perfect staggering due to steric interactions.

Discussion

The solution and solid-state properties of polymers are determined by their conformational characteristics on the molecular level. For this reason, the experimental and theoretical properties of polymers have been extensively studied. In solution the three-bond proton–proton coupling constants, dipole moment measurements, and end-to-end distances have been measured,[1,2] and the values from these studies are frequently compared with those from theoretical studies, such as RIS calculations.[33-36] In this study we show another approach toward determining the structure of polymers in solution. Here we measure the strength of the dipolar interaction between main-chain protons and relate them to the interatomic distances, which set limits on the possible contributions of the tt, tg^-, and g^+t states to the average solution conformation.

NMR relaxation is particularly useful for the determination of the local conformation because the relaxation rates are inversely proportional to the sixth power of the proton separation. Therefore, strong interactions are expected for separations of 2–3 Å only. Due to the limited number of measurable interactions (four), however, it is not possible to directly solve the structure, and certain assumptions must be made. Here we assume that the average solution conformation is an average of the tt, tg^-, and g^+t states. Theoretical studies suggest that this is a reasonable assumption.[33-36] We also assume equal deviations of ϕ_1 and ϕ_2 from the classical gauche and trans states. We believe this assumption reasonable since the same types of steric interactions are responsible for the deviations about ϕ_1 and ϕ_2.[15] Also implicit in our analysis is the assumption that the distances average in a simple way. We believe these assumptions are justified because the jumps between conformers are considerably faster than the overall chain–chain motion[29,37] (~0.5 ns) that modulates the dipolar interactions.

The conformational picture emerging from these studies differs in some details from the RIS models. The RIS and experimental data presented here agree that the solution conformation is predominately tt with approximately equal mixtures of tg^- and g^+t. The difference between the two approaches is in the exact amount of tg^- and g^+t. The difference may be due either to experimental variables or to assumptions within the RIS model that approximates the copolymer interactions as the average of those for polystyrene and poly(methyl methacrylate). The NMR data also suggest that the isomeric states are staggered by 11° to relieve crowding of the bulky groups. This value is intermediate between that for polystyrene and poly(methyl methacrylate).

2D NMR has been extensively used for structure determination in biopolymers[7,9-11] but has seen no application towards the conformational properties of synthetic polymers. Synthetic polymers differ from biological ones in that they are usually not rigid and, in many cases, have a statistical rather than a specific monomer sequence. The conformational information is obtained from the analysis of the through-space dipolar interactions. This analysis is not unique to 2D NMR; the rates obtained from this analysis are the same as those in 1D NMR studies. The advantages of the 2D approach are that the spins are labeled via their precessional frequencies rather than by selective pulses and that all interactions can be probed within a single spectrum.[17-19] The disadvantages of the 2D approach are the amount of time required (18 h per spectrum) and the massive amount of data generated.

In conclusion, the 2D NMR analysis can provide a detailed picture of the average solution conformation of the alternating 1:1 styrene–methyl methacrylate copolymer. From the distances measured by NMR we can determine the populations of isomeric states and the deviation from perfect staggering. The ability to reach such detailed conclusions is due in part to the fact that the conformation can be determined by measuring local interactions. NMR is particularly sensitive to these types of interactions. Further studies are in progress which may lead to the application of these techniques to a wide variety of conformationally averaging natural and synthetic polymers.

Registry No. (Styrene)(methyl methacrylate) (alternating copolymer), 108266-99-5.

References and Notes

(1) Bovey, F. A. *Chain Structure and Conformation of Macromolecules*; Academic: New York, 1982.
(2) Bovey, F. A.; Winslow, F. H. *Macromolecules, An Introduction to Polymer Science*, Academic: New York, 1979.
(3) Flory, P. J. *Statistical Mechanics of Chain Molecules*; Wiley-Interscience: New York, 1969.
(4) Bovey, F. A. *High Resolution* NMR *of Macromolecules*; Academic: New York, 1972.
(5) Komoroski, R. A. *High Resolution NMR Spectroscopy of Synthetic Polymers in Bulk*; VCH Publishers Inc., 1986.

(6) Bruch, M. D.; Bovey, F. A.; Cais, R. E. *Macromolecules* **1984**, *17*, 2547.
(7) Macura, S.; Brown, L. R. *J. Magn. Reson.* **1983**, *53*, 529.
(8) Bruch, M. D.; Bovey, F. A. *Macromolecules* **1984**, *17*, 978.
(9) Mirau, P. A.; Bovey, F. A. *Macromolecules* **1986**, *19*, 210.
(10) Young, G. B.; James, T. L. *J. Am. Chem. Soc.* **1984**, *106*, 7986.
(11) Gondal, D.; Van Binst, G. *Biopolymers* **1986**, *25*, 977.
(12) Bruch, M. D.; Noggle, J. H.; Gierasch, L. M. *J. Am. Chem. Soc.* **1985**, *107*, 1400.
(13) Wider, G.; Macura, S.; Kumar, A.; Ernst, R. R.; Wuthrich, K. *J. Magn. Reson.* **1984**, *56*, 207.
(14) Kearns, D. R. *CRC Crit. Rev. Biochem.* **1985**, *15*, 237.
(15) Heffner, S. A.; Bovey, F. A.; Verge, L. A.; Mirau, P. A; Tonelli, A. E. *Macromolecules* **1986**, *19*, 1628.
(16) States, D. J.; Haberkorn, R. A.; Ruben, D. J. *J. Magn. Reson.* **1982**, *45*, 286.
(17) Jeneer, J.; Meier, B. H.; Bachman, P.; Ernst, R. E. *J. Chem. Phys.* **1979**, *71*, 4546.
(18) Macura, S.; Ernst, R. E. *Mol. Phys.* **1980**, *41*, 95.
(19) Olejniczak, T. E.; Hoch, J. E.; Dobson, C. M.; Poulson, F. M. *J. Magn. Reson.* **1985**, *64*, 199.
(20) Blouin, F. A.; Cheng, R. C.; Quinn, M. M.; Harwood, H. J. *Polym. Prepr. (Am. Chem. Soc., Div. Polym. Chem.)* **1973**, *14*, 25.
(21) Hirai, H.; Tanabe, T.; Koinuma, H. *J. Polym. Sci., Polym. Chem. Ed.* **1979**, *17*, 843.
(22) Koinuma, H.; Tanabe, T.; Hirai, H. *Macromolecules* **1980**, *18*, 383.
(23) Schilling, F. C.; Bovey, F. A.; Bruch, M. D.; Kozlowski, S. A. *Macromolecules* **1985**, *18*, 1418.
(24) Macura, S.; Wuthrich, K.; Ernst, R. E. *J. Magn. Reson.* **1982**, *47*, 351.
(25) Ellena, J. F.; Hutton, W. C.; Cafiso, D. S. *J. Am. Chem. Soc.* **1985**, *107*, 1530.
(26) Olejniczak, E. T.; Gampe, R. T.; Fasik, S. *J. Magn. Reson.* **1986**, *67*, 28.
(27) Perrin, C. L.; Gipe, R. E. *J. Am. Chem. Soc.* **1984**, *106*, 4036.
(28) Massefski, W.; Bolton, P. H. *J. Magn. Reson.* **1985** *65*, 526.
(29) Keepers, J. W.; James, T. L. *J. Magn. Reson.* **1984**, *57*, 404.
(30) Heatley, F. *Prog. NMR Spectrosc.* **1980**, *13*, 47.
(31) Bovey, F. A.; Jelinski, L. W. *J. Phys. Chem.* **1985**, *89*, 571.
(32) Schilling, F. C. *Macromolecules* **1978**, *11*, 1290.
(33) Koinuma, H.; Tanabe, T.; Hirai, H. *Makromol. Chem.* **1980**, *181*, 383.
(34) Yoon, D. Y.; Sundararajan, P. R.; Flory, P. J. *Macromolecules* **1975**, *8*, 776.
(35) Yoon, D. Y.; Suter, V. W.; Sundararajan, P. R.; Flory, P. J. *Macromolecules* **1975**, *8*, 784.
(36) Sundararajan, P. R. *J. Polym. Sci., Polym. Lett. Ed.* **1977**, *15*, 699.
(37) Tropp, J. *J. Chem. Phys.* **1980**, *72*, 6036.

Intramolecular Compartmentalization of Photoredox Centers in Functionalized Amphiphilic Polyelectrolytes: A Model for Collisionless Electron Transfer Systems

Yotaro Morishima,* Takaomi Kobayashi, Toshiaki Furui, and Shun-ichi Nozakura

Department of Macromolecular Science, Faculty of Science, Osaka University, Toyonaka, Osaka 560, Japan. *Received December 10, 1986*

ABSTRACT: Photoactive centers (phenanthryl groups) covalently linked to a polyanion were "compartmentalized" in the hydrophobic aggregates of pendant phenyl groups covalently incorporated in the polyanion. In this amphiphilic polyanion, a collisionless long-range electron transfer occurs from photoexcited phenanthrene (Phen) moieties to methylviologen (MV^{2+}) bound electrostatically as well as hydrophobically to the peripheral area of the hydrophobic aggregates. Backreaction also takes place in a collisionless process. Without pendant phenyl groups, the Phen residues tend to form ground-state charge-transfer (CT) complexes with MV^{2+}, which highly disfavor the photochemical production of $MV^{\bullet+}$. As a result of the compartmentalization, the CT complexation with MV^{2+} was suppressed while the Phen fluorescence quenching was enhanced, leading to a considerable increase in the photochemical yield of $MV^{\bullet+}$. An important observation was that the back electron transfer was slower than the forward reaction by a factor of at least 10^3, which may be explicable in terms of the "inverted region" of electron transfer theory proposed by Marcus and others. Pendant lauryl chains in place of phenyl groups were found to be ineffective in compartmentalizing the Phen moieties presumably because the aggregates of long alkyl chains are loose as compared to those of aromatic rings that tend to stack tightly in the aggregates.

Introduction

For an understanding of the fundamental aspect of collisionless electron-transfer reactions that are known to be operating in biological photosynthetic systems,[1] considerable interest has been directed toward simple model systems in which electron donors and acceptors are tightly held in fixed distances so that no diffusional encounter of the reactants is allowed. These model systems include rigid matrix systems, wherein the reactant molecules are buried in separation,[2] and linked donor–acceptor molecules with a rigid spacer.[3] A large number of studies have also focused on electron-transfer processes across the interfaces of some organized assemblies such as surfactant micelles and vesicles, where some particular donors and acceptors are expected to reside separately with respect to a phase boundary. However, in these interfacial systems, it is difficult to fix the reactants in a specific location because of the dynamic nature of the systems.

Amphiphilic polyelectrolytes have been demonstrated to form organized structures as a result of intramolecular microscopic phase separations in aqueous media consisting of aggregates of the hydrophobic residues and of charged interfaces.[4-6] Previous papers have shown that an amphiphilic copolymer of 9-vinylphenanthrene (9VPh) and 2-(acrylamido)-2-methylpropanesulfonic acid (AMPS) behaves as an unimolecularly organized assembly with photochemical functionality.[7-11] Phenanthrene (Phen) residues covalently linked to the amphiphilic copolymer form a tight ground-state complex with methylviologen (MV^{2+}) as a consequence of electrostatic, hydrophobic, and

0024-9297/87/2220-1707$01.50/0